Int J Thermophys (2009) 30:155–166
DOI 10.1007/s10765-008-0473-2

Optical Diffraction Corrections in Radiometric Thermodynamic Temperature Determination

S. Briaudeau · B. Rougié · M. Sadli · A. Richard · J. M. Coutin

Published online: 4 December 2008

Abstract One of the main components of uncertainty in high-temperature thermometry arises because of the size-of-source effect (SSE). This effect makes the temperature measurement sensitive to the geometry of the radiating environment. It is caused by optical diffraction and especially by light scattering off/from, and interreflections between, optical components inside the pyrometer. The LNE-INM/CNAM is involved in extending the thermometry temperature scale to very high temperatures ($T > 2000\,^{\circ}\mathrm{C}$) and has developed eutectic-based fixed points (Sadli et al. (in: Zvizdic (ed.) Proceedings of TEMPMEKO 2004, 9th International Symposium on Temperature and Thermal Measurements in Industry and Science, 2004)) and a thermodynamic temperature measurement capability based on absolute radiometric methods (Briaudeau et al. (in: D. Zvizdic (ed.) Proceedings of TEMPMEKO 2004, 9th International Symposium on Temperature and Thermal Measurements in Industry and Science 2004)). A new measurement technique that uses an optical fiber has been developed and tested, allowing the determination of the SSE at any defocusing plane, with high resolution. A model based on optical diffraction has been developed to simulate the SSE in a real situation, considering the contribution to the pyrometer signal of the whole "3D" optical scene inside the blackbody furnace. Using the same approach, it has been demonstrated that optical scattering in a simple radiance meter can be estimated from accurate optical diffraction measurement.

Keywords Blackbody · Diffraction · High temperature · ITS-90 · Optical fiber · Radiance · Radiometry · Size-of-source effect · Thermometry · Thermodynamic temperature

S. Briaudeau (✉) · B. Rougié · M. Sadli · A. Richard · J. M. Coutin
Institut National de Métrologie-Laboratoire National d'Essais, Conservatoire National des Arts et Métiers (INM-LNE/CNAM), 61 rue du Landy, 93210 La Plaine Saint Denis, France
e-mail: briaudeau@cnam.fr

1 Introduction

At high temperatures ($T > 900\,\mathrm{K}$), the most accurate temperature measurement is made by measurement of optical radiation [2–4]. At 1357.77 K (the copper point), the typical measurement uncertainty is about 0.1 K.

This paper explores both the theoretical and experimental aspects of the size-of-source effect optical signal correction. The "SSE" is related to the sensitivity of the optical instrument signal to the size of the optical source imaged. Due to this effect, the pyrometer signal depends on the optical scene surrounding the optical target viewed, and it has to be corrected. A pyrometric comparison of the temperature of two similar blackbodies will reduce the SSE correction as there is partial cancellation. In the case of thermodynamic temperature measurement as used at INM, the radiance of the studied blackbody is compared to that from an integrating sphere (which provides a monochromatic radiance etalon) [5]. In this case, the optical scene geometries show very different shapes and sizes; thus, the SSE correction is not mitigated and its estimation with an uncertainty below 10 % becomes critical.

The SSE has been experimentally studied by several authors [4,6–10]. Two classical methods called "direct" and "indirect" are used to measure the SSE [6]. As an alternative, a new method to measure the "SSE" using an optical fiber source is described in the first section of this paper. The first experimental results obtained are discussed and compared to the usual method. In the second section, the "SSE" observation method is elaborated theoretically by optical diffraction theory and numerically simulated, depending on the optical characteristics of the pyrometer. In the third section, experiments show that the study of the optical diffraction correction of our radiancemeter signal allows us to reduce the inter-reflections (and hence SSE) of the radiance measurement signal.

2 New "SSE" Measurement Method Using an Optical Fiber

The SSE is defined as the pyrometer signal viewing a circular optical source of radiance L and diameter R divided by the pyrometer signal viewing a radiating source of quasi-infinite spatial extent with the same radiance L: $\mathrm{SSE_T}(R) = S(R)/S(R \to \infty)$. For practical purposes, one defines a "Truncated SSE": $\mathrm{SSE_T}(R) = \mathrm{S}(R)/\mathrm{S}(R_{\mathrm{Max}})$ where R_{Max} replaces $R \to \infty$. The SSE is classically measured with an integrating sphere, which provides a variable-radius optical source. The "direct" method suffers from a strong uncertainty as the sphere output radiance cannot be kept constant because it depends on its output port external radius. This is why in most direct method determinations a blackbody reference source with a variable-aperture system is used. In the indirect method, the central region of the sphere output is occulted by an optical mask of radius R_{Min} so that the pyrometer signal recorded becomes $S_{\mathrm{ind}}(R) = S(R) - S(R_{\mathrm{Min}})$ and the SSE becomes

$$\mathrm{SSE}_T(R) = 1 - \left[\frac{S_{\mathrm{ind}}(R_{\mathrm{Max}}) - S_{\mathrm{ind}}(R_{\mathrm{Min}})}{S(R_{\mathrm{Min}})}\right].$$

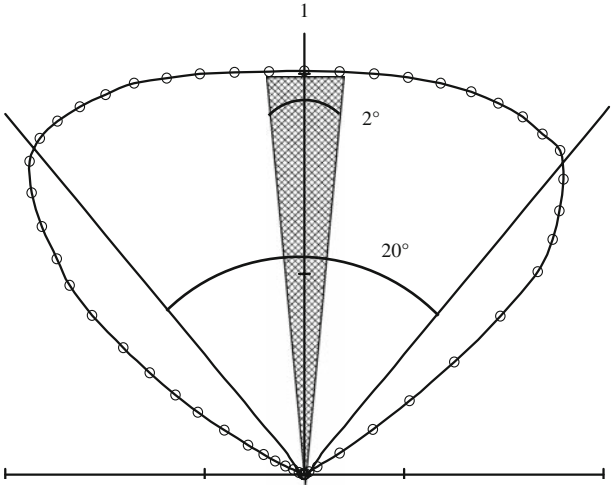

Fig. 1 Angular distribution of the optical fiber output radiance

The new SSE measurement method presented in this paper uses a laser-injected multimode optical fiber as a "point-like" optical source whose position is translated. The multimode fiber is agitated to mitigate the speckle effect. The pyrometer tested is composed of a thin lens limited by a circular aperture (pupil), a field stop, a Czerny-Turner monochromator, and a photodetector. The pyrometer viewing angle is about 2° around its optical axis. The angular distribution of the optical fiber radiance can be considered quasi-Lambertian over 10° around the optical axis (see Fig. 1). As the pyrometer viewing angle is only about 1° around the optical axis, the optical fiber provides a quasi-Lambertian optical source. Due to optical diffraction, the image of the fiber tip cannot be considered a point image; instead, an Airy pattern is generated depending on the pyrometer optical parameters. A pyrometer of focal distance $f_0 = 50\,\text{cm}$, with an f-number $f_0/20$, and a magnification $M = \frac{d_\text{i}}{d_\text{o}} = 1$ (d_i is the object–lens distance and d_0 is the lens-image distance) gives an Airy pattern of radius $R_\text{A} \approx 50\,\mu\text{m}$ at a wavelength $\lambda = 800\,\text{nm}$. For these conditions, a 50 μm diameter optical fiber produces a 50 μm diameter diffraction pattern, which is not negligible but still remains small compared to the field-stop radius used in the pyrometer under consideration ($R_\text{i} = 1\,\text{mm}$). As our optical fiber delivers a 10 mW laser beam over an angle of 10° around the optical axis, 1 % (0.1 mW) of the fiber output optical power enters the pyrometer. When the optical fiber end is situated at the center of the image of the field stop, the optical power reaches its maximum level in the linear regime of silicon photodiodes, allowing the SSE measurement to be determined over a very high dynamic range.

Translating the optical fiber along the pyrometer field of view provides a measurement of the pyrometer spatial impulse response function $S_\text{Fiber}(x, y, z)$ in the "z" plane where z is the defocusing distance. The experimental setup is shown in Fig. 2. The signal of the pyrometer focusing the optical fiber tip on its field stop provides a reference that is recorded between each measurement. With these conditions, the drift of

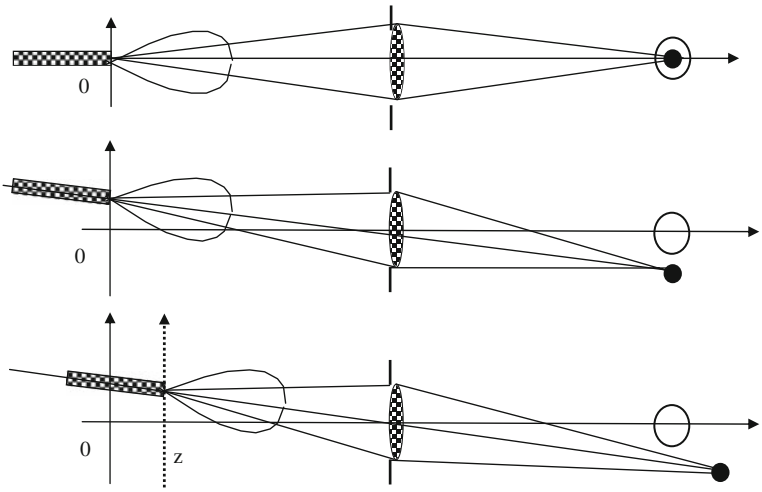

Fig. 2 Experimental setup used to measure the pyrometer size-of-source effect with an optical fiber (**a**) the image of the optical fiber tip is centered on the field stop, (**b**) the image of the optical fiber tip is blocked by the field stop, (**c**) the image of the optical fiber tip is defocused and blocked by the field stop

the optical fiber output power was measured to be less than 0.5 % between two measurements and the correction of this drift was realized with 0.02 % uncertainty, including the pyrometer response drift. An example of a recorded profile $S_{\mathrm{Fiber}}(x, y, z = 3.5\ \mathrm{cm})$ is shown in Fig. 3. In this example, the field stop radius is 1.25 mm and the defocusing z = 3.5 cm. The pyrometer output sensitivity is six orders of magnitude smaller 1 cm away from its field of view center. In this example, the signal-to-noise ratio is better than 10^6. To a first approximation, the optical target viewed by the pyrometer remains cylindrical, although defocused. Thus, it is possible to integrate numerically the pyrometer signal recorded $S_{\mathrm{Fiber}}(r, z)$ and to compute its response to a hypothetical circular optical source of radius r: $\mathrm{SSE}_{\mathrm{Fiber}}(r, z) = 2\pi \int_0^r S_{\mathrm{Fiber}}(x, y, z)x\mathrm{d}x$. The pyrometer SSE computed from the optical fiber experiment $\mathrm{SSE}_{\mathrm{Fiber}}(r, z)$ is shown in Fig. 4. This result shows the very good signal-to-noise ratio of the SSE computation with this experimental method. This experimental method has other advantages: the optical source is monochromatic, very stable, its geometry is kept constant, and the distance of the fiber position to the field-stop center can be much greater than that with an integrating sphere.

3 Simulation of "3D SSE" from Optical Diffraction Computation

To obtain very flat freezing plateaux (about 10 mK at 1357.77 K [Cu point]) with an ITS-90 fixed point, the blackbody crucible must experience a very small temperature gradient. This is obtained through the use of thermal screens distributed inside the oven, along the optical axis. The contribution of these radiating thermal screens to the pyrometer signal has been estimated using this methodology by computing the

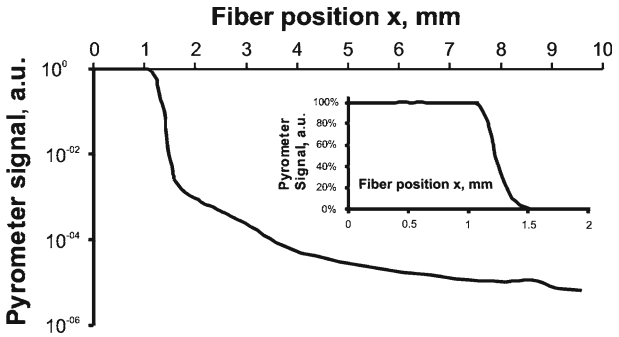

Fig. 3 Pyrometer signal as a function of the optical fiber position

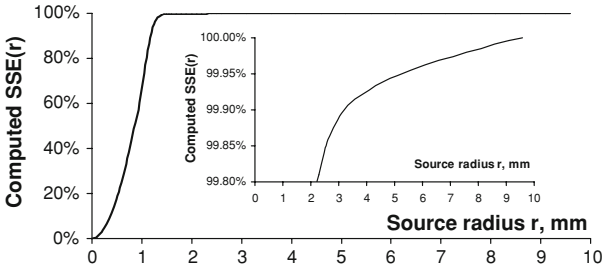

Fig. 4 Size-of-source effect computed from optical fiber measurements

pyrometer response to any circular optical source, at any defocusing (see Fig. 5), following a physical model based on optical diffraction theory [11]. The pyrometer considered is simply composed of a focusing lens, limited by a pupil, and a field stop. An annular configuration of the optical source is simply obtained by subtracting the contribution of two Lambertian circular optical sources having the same irradiance but radii equal to the external and internal radii of the annulus, respectively.

The pyrometer can be assumed to be a linear instrument invariant under translation. The object image is the convolution product of the object and the impulse response function of the pyrometer (Airy pattern). In the paraxial approximation, the pyrometer imaging system can be analyzed using Fourier optics (or optical diffraction). In the spatial frequency domain, the image intensity spectrum $I_{\mathrm{i}}(f)$ (spatial frequency f) simply results from the linear filtering of the object intensity spectrum $G_{R_{\mathrm{o}}}(f)$ with the pyrometer optical transfer function (OTF(f)): $I_{\mathrm{i}}(f) = \mathrm{OTF}(f) G_{R_{\mathrm{o}}}(f)$.

In the Fraunhoffer approximation, the OTF of the pyrometer viewing an incoherent optical source is expressed as [10]

$$\mathrm{OTF}_z(f_x, f_y) = \frac{C}{\lambda^2 (d_0 + z)^2 d_{\mathrm{i}}^2} \iint P\left(x + \frac{\lambda d_{\mathrm{i}} f_x}{2}, y + \frac{\lambda d_{\mathrm{i}} f_y}{2}\right) \times P\left(x - \frac{\lambda d_{\mathrm{i}} f_x}{2}, y - \frac{\lambda d_{\mathrm{i}} f_y}{2}\right) \mathrm{d}x\mathrm{d}y$$

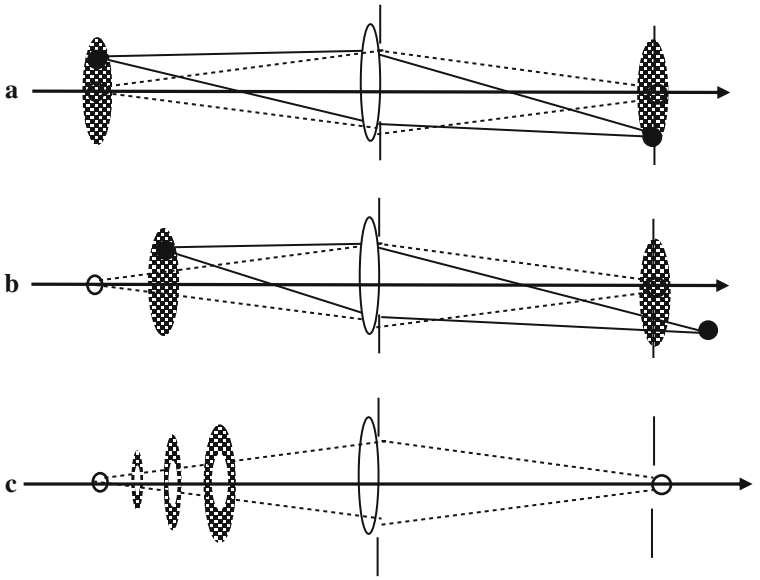

Fig. 5 Experimental layout considered for the computation of the out-of-focus size-of-source effect (**a**) in-focus SSE, (**b**) out-of-focus SSE, and (**c**) oven configuration

where λ is the optical wavelength considered, d_0 is the field stop-lens distance, d_i is the lens-image distance, z is the defocusing distance of the optical source considered, and C is a constant.

$P(x, y, z) = P_{\text{Focus}}(x, y)\mathrm{e}^{iW(x,y,z)}$ is the circular stop aperture complex function at a defocusing distance z. At $z = 0$, it reduces to the pupil function,

$$P_{\text{focus}}(x, y) = 1 \text{ if } \sqrt{x^2 + y^2} \leq a \text{ and } P_{\text{focus}}(x, y) = 0 \text{ if } \sqrt{x^2 + y^2} \geq a$$

where a is the entrance pupil radius.

$W(x, y, z) = \pi \frac{\varepsilon(z)}{\lambda}(x^2 + y^2)$ is the wave-front aberration function versus defocusing distance z.

$\varepsilon(z) = \frac{1}{d_0+z} + \frac{1}{d_\text{i}} - \frac{1}{f_\text{I}}$ is a defocusing function with f_I the lens focusing distance so that an optical source situated in the field stop conjugate plane gives $\varepsilon(z = 0) = 0$.

In the focal plane ($z = 0$ so that $\varepsilon(z = 0) = 0$ and $P(x, y, z = 0) = P_{\text{focus}}(x, y)$), the "OTF" reduces to a simple analytical expression in cylindrical coordinates [10]:

$$\text{OTF}_{z=0}(f) = \frac{4aC}{\lambda^2(d_0 + z)^2 d_\text{i}^2} \int_0^{a(1-\frac{f}{f_\text{c}})} \sqrt{1 - \left(\frac{x}{a} + \frac{f}{f_\text{c}}\right)^2}\,\mathrm{d}x$$

$$\text{OTF}_{z=0}(f) = \frac{2a^2C}{\lambda^2(d_0 + z)^2 d_\text{i}^2} \left[\arccos\left(\frac{f}{f_\text{c}}\right) - \left(\frac{f}{f_\text{c}}\right)\sqrt{1 - (\frac{f}{f_\text{c}})^2}\right]$$

with $f_\text{c} = \frac{2a}{\lambda d_\text{i}}$, the pyrometer spatial cut-off frequency.

Out of the focal plane ($z \neq 0$), the "OTF" reduces to a simple integral thanks to the cylindrical symmetry of the aberration function $W(z, x, y)$ and of the stop aperture $P_{\text{focus}}(x, y)$:

$$\text{OTF}_z(f) = \frac{4aC}{\lambda^2(d_0+z)^2 d_\text{i}^2} \int_0^{a\left(1-\frac{f}{f_\text{c}}\right)} \sqrt{1-\left(\frac{x}{a}+\frac{f}{f_\text{c}}\right)^2} \cos\left(2\pi \frac{\varepsilon(z) d_\text{i}}{2}\right) f(x)\text{d}x$$

The object spatial frequency $G_{R_\text{o}}(f)$ spectrum is the "2D" Fourier transform of a disk of radius R_o;

$$G_{R_\text{o}}(f) = 2\pi I_0 \int_0^{R_\text{o}} J_0(2\pi f r) r \text{d}r = I_0(2\pi R_\text{o}^2) \frac{J_1(2\pi R_\text{o} f)}{(2\pi R_\text{o} f)}$$

where $J_1(x)$ is the Bessel function of the first kind.

Then, the image intensity distribution $I_\text{i}(r, R_\text{o}, z)$ in the field stop plane can be expressed as the inverse Fourier transform of the filtered object spectra by the pyrometer, depending on the pyrometer optical parameters and the object defocusing.

$$I_\text{i}(r, R_\text{o}, z) = 2\pi \int_0^{+\infty} \text{OTF}_z(f) G_{R_\text{o}}(f)\ J_0(2\pi f r)\ f \text{d}f$$

where $J_0(x)$ is the Bessel function of the zeroth kind.

The optical flux $\phi(R_\text{i}, R_\text{o}, z)$ passing through the field stop of radius R_i can be expressed as

$$\phi(R_\text{i} R_\text{o}, z) = 2\pi \int_0^{R_\text{i}} I_\text{i}(r, R_\text{o}, z)\ r \text{d}r = 2\pi R_\text{i} \int_0^{+\infty} \text{OTF}_z(f) G_{R_\text{o}}(f) J_1(2\pi f R_\text{i})\ \text{d}f$$

The last two formulae have been applied to simulate the diffraction contribution to the size-of-source effect in or out of the focal plane.

The optical diffraction computation shows some optical behavior that cannot be explained by geometrical optics, such as the Airy-pattern dependence on defocusing, shown in Fig. 6. The optical diffraction model described above has been used to compute the pyrometer signal when viewing a circular source of variable diameter at a defocusing distance z. Under these conditions, the pyrometer signal is nothing else but the pyrometer SSE observation signal fully explained by optical diffraction. As an example, Fig. 7 shows the computation of the size-of-source effect observed with a circular source of variable diameter, positioned at two different defocusing distances ($z = 0$ and $z = -20\,\text{cm}$), having a focal distance $f_\text{I} = 0.5\,\text{m}$, a focusing distance $d_\text{i} = d_0 = 1\,\text{m}$, and a field stop radius $R_0 = 1\,\text{mm}$. This computation shows that

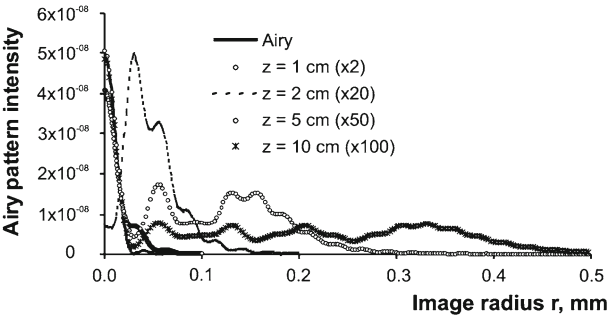

Fig. 6 Diffraction pattern computed at different defocusing distances ($z = 0$, $z = 2\,\text{cm}$, and $z = 5\,\text{cm}$)

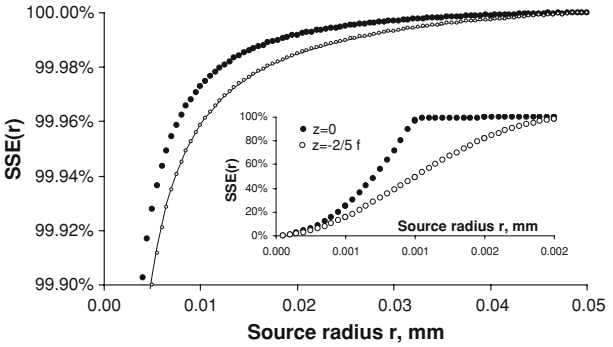

Fig. 7 Size-of-source effect computed from optical diffraction at two defocusing distances ($z = 0$ and $z = -25\,\text{cm}$)

defocusing destroys the optical performance and enhances the optical diffraction as well as the SSE.

This optical diffraction description has been used to compute the contribution of thermal screens of uniform temperature and distributed along the furnace optical axis following a conical geometry and exhibiting an annular geometry:

$$R_{\text{int}}(z=0)=0;\;\; R_{\text{int}}(z=l)=R_{\max}$$
$$R_{\text{int}}\left(z_{\text{i}}=i\,\frac{l}{N}\right)=i\,\frac{R_{\max}}{N}$$
$$R_{\text{ext}}(z_{\text{i}})=R_{\text{int}}(z_{\text{i}})+R_0$$

The contribution to the pyrometer signal of these "out-of-focus" screens ($l = 10\,\text{cm}$, $R_{\max} = 5\,\text{cm}$, and $N = 50$) has been plotted in Fig. 8. In this example, the screens' contribution is about 0.1 %, which is far from negligible in a thermodynamic temperature measurement uncertainty budget. The optical diffraction computation gives the theoretical lower limit of the size-of-source effect for any optical diffraction-limited imaging system. It does not include the contribution of optical diffusion from the optical surfaces.

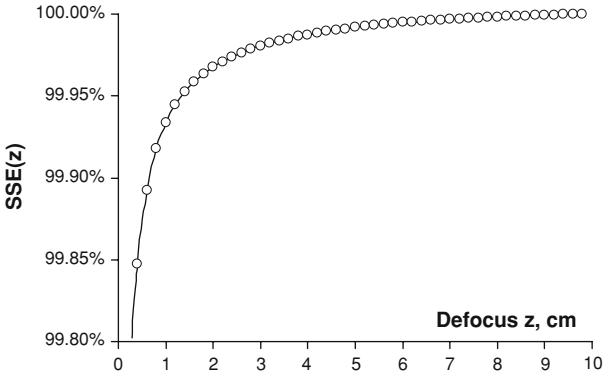

Fig. 8 Size-of-source effect computed from diffraction caused by "out-of-focus" radiating thermal screens distributed along the pyrometer optical axis

4 Inter-reflections and Optical Diffraction Measurements

The LNE INM/CNAM developed its own radiance meter for thermodynamic temperature measurement a few years ago [5]. It consists of a precise mechanical positioning of a radiometer in front of a monochromatic, uniform, and Lambertian radiance source that is made using a laser injected into an integrating sphere. The radiometer is made of a precise diaphragm and a silicon trap-detector calibrated against a cryogenic radiometer. The experimental setup used is shown in Fig. 9. The integrating-sphere output is defined by a precisely machined diaphragm of the same radius ($R_0 = 3\,\text{mm}$) as that of the radiometer. In the experiments presented here, a tunable, but low optical power, extended-cavity diode laser (10 mW) was used; thus, the distance d separating the radiometer from the integrating sphere was reduced to $d = 31\,\text{cm}$ to optimize the signal-to-noise ratio [5].

The main error in this radiance measurement setup was caused by optical inter-reflections between the circular plates of radius R_{out} that maintain the two diaphragms in the correct position and are separated by a specific distance. Following a very approximate computation, the fraction F_{ϕ_0} of the detected optical flux ϕ_0 coming from inter-reflections is

$$F_{\phi_0} = \frac{\phi_\rho}{\phi_0} = \rho^2 \left(\frac{R_{\text{out}}}{d} \right)^4 ,$$

where ρ is the mean material diffusivity (here $\rho = 1$). As the optical power available was too low, it was not possible to make d vary more than 3 cm; this should make F_{ϕ_0} change by only 60 %, which is difficult to detect as $F_{\phi_0} \ll 1$ and the optical flux ϕ_0 is also expected to change by 25 % at the same time.

Using the same approximate computation, it is possible to reduce the inter-reflections by simply inserting a baffle (internal radius $R_{\text{baffle}} = yR_0$ $(1 < y)$, external radius R_{out}, and diffusivity ρ) placed at a distance $z = xd$ $(0 < x < 1)$ from the integrating sphere (Fig. 9b, c). In the approximation used, one considers only the principal optical

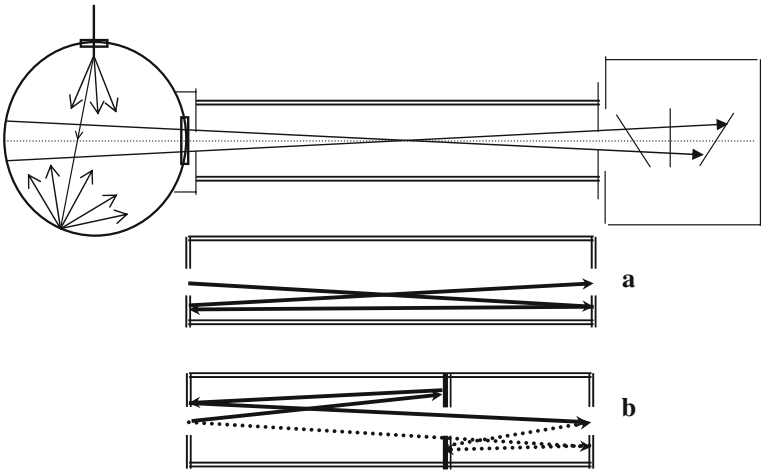

Fig. 9 Experimental setup of the radiance meter used to estimate its diffraction and diffusion corrections (**a**) inter-reflections on diaphragm screens, (**b**) inter-reflections induced by the baffle)

rays originating from the center of the source (i.e., detector) and intercepting the baffle disk until the next reflecting surface. Thus, the fraction of the light flux coming from inter-reflections and entering the detector becomes

$$F_{\phi_0}(x, y) = \rho^2 \frac{R_{\text{out}}^2 R_0^2}{d^4} \left[\frac{\left(\frac{y}{x}\right)^2 - 1}{(1-x)^4} + \frac{\left(\frac{y}{1-x}\right)^2 - 1}{x^4} \right].$$

Theoretically, the best position to place this diaphragm is obtained for $z = d/2$, although the best position found experimentally is $z = d/3$. One adverse consequence of introducing this new diaphragm is a new source of optical diffraction that enhances the radiance meter signal as the diaphragm radius decreases, as computed from optical diffraction theory using the "NIST computer program for diffraction corrections in radiometry." This computation is based on the Born and Wolf textbook that treats Fresnel optical diffraction using Lommel functions. Following these two models, the optical inter-reflections remain negligible compared to the optical diffraction (as shown in Fig. 10). The radiance measurements were made with a baffle of variable diameter positioned at several distances from the integrating sphere source, injected either with a laser or with an LED, in order to observe any coherence effect. As shown in Fig. 11, there is no evidence of a coherence effect, as the LED and laser curves are about the same. The optical diffraction computation fits approximately the experimental curves measured, although the disagreement increases as the radius tends to the detector (and source) radius R_0. The computed optical diffraction is a minimum at $z = d/3$ or $z = 2d/3$, which corresponds approximately to the experimental results obtained. In conclusions, the inter-reflections seem to be negligible in the presence of the baffle that should be placed at $z = d/3$ and whose diameter must be at least 10 mm to reduce the diffraction correction to about 0.05 %.

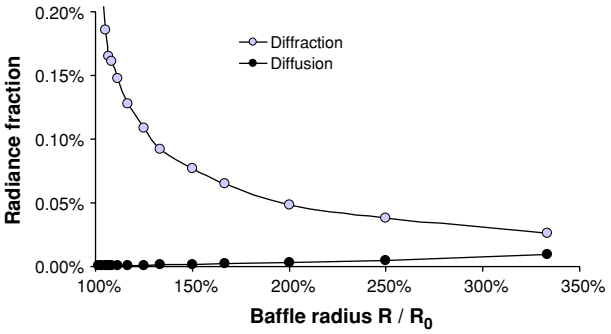

Fig. 10 Diffraction measurement of radiance meter; comparison to simulation

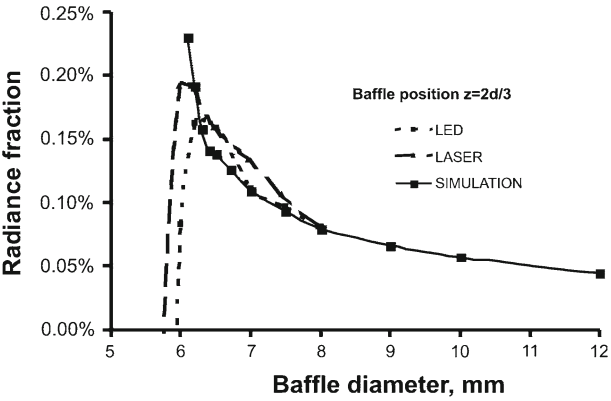

Fig. 11 Simulation of the radiance excess coming from (**a**) diffraction and (**b**) inter-reflections

5 Conclusion

This new SSE measurement method uses an optical fiber and offers very high resolution as well as the capability to map the SSE at any defocusing distance and at very large diameters. The pyrometer signal has been estimated from an optical diffraction model, and the results broadly agree with the experimental SSE data recorded with similar optical parameters.

The optical diffraction certainly does not completely explain the SSE, but it gives a theoretical lower limit for any diffraction-limited optical instrument. This model can also be used to estimate the contribution of any out-of-focus thermal screen, or to simulate the pyrometer signal when viewing a 3D radiating object. The computational principle can be extended to more complex pyrometers, including one with a Lyot stop. Our approach, based on optical diffraction computation, provides a useful tool to estimate the real optical performance of the pyrometer in the diffraction limit. The difference between the real pyrometer response and the optical diffraction model can provide an estimate of the upper limit of optical scattering or inter-reflections inside the pyrometer.

Optical baffles can be used to discriminate between optical diffraction and optical inter-reflections occurring in a "two-diaphragm radiance meter," as the minimum correction is obtained at very different positions of the baffle, depending on the optical process from which the detected stray light originates.

Acknowledgments One of the authors (S. B.) thanks H. Yoon for his help, lending a NIST optical diffraction program used in the third section of this paper.

References

1. M. Sadli, F. Bourson, M. Fanjeaux, S. Briaudeau, B. Rougie, G. Bonnier, in *Proceedings of TEMPMEKO 2004, 9th International Symposium on Temperature and Thermal Measurements in Industry and Science*, ed. by D. Zvizdic (FSB/LPM, Zagreb, Croatia, 2004), pp. 611–620
2. K. Anhalt, J. Hartmann, D. Lowe, G. Machin, M. Sadli, Y. Yamada, Metrologia **43**, S78 (2006)
3. R. Goebel, Y. Yamada, M. Stock, in *Proceedings of TEMPMEKO 2004, 9th International Symposium on Temperature and Thermal Measurements in Industry and Science*, ed. by D. Zvizdic (FSB/LPM, Zagreb, Croatia, 2004), pp. 91–99
4. D. Lowe, M. Battuello, G. Machin, F. Girard, in *Temperature, Its Measurement and Control in Science and Industry*, vol. 7, ed. by D.C. Ripple (AIP, New York, 2003), pp. 625–630
5. S. Briaudeau S. Briaudeau, B. Rougié, M.Fanjeaux, M.Sadli, G. Bonnier, A. Richard, J.M. Coutin, J. Bastie, in *Proceedings of TEMPMEKO 2004, 9th International Symposium on Temperature and Thermal Measurements in Industry and Science*, ed. by D. Zvizdic (FSB/LPM, Zagreb, Croatia, 2004), pp. 119–125
6. P. Bloembergen, Y. Duan, R. Bosma, Z. Yuan, in *Proceedings of TEMPMEKO '96, 6th International Symposium on Temperature and Thermal Measurements in Industry and Science*, ed. by P. Marcarino (Levrotto and Bella, Torino, 1997), pp. 261–266
7. G. Machin, M. Ibrahim, in *Proceedings of TEMPMEKO'99, 7th International Symposium on Temperature and Thermal Measurements in Industry and Science*, Vol. II, ed. by J.F. Dubbeldam, M.J. de Groot (NMi-VSL, Delft, The Netherlands, 1999), pp. 681–686
8. H.W. Yoon, Metrologia **43**, S22 (2006)
9. H.W. Yoon, D.W. Allen, R.D. Saunders, Metrologia **42**, 89 (2005)
10. J.W. Goodman, *Introduction to Fourier Optics*, 3rd edn. (Roberts & Company Pub., Greenwood Village, Colorado, 2004)
11. M. Born, E. Wolf, *Principles of Optics*, 6th edn. (Pergamon Press, New York, 1987)